1 **Calcium entry does not drive fast mechanotransduction adaptation in cochlear**
2 **hair cells**
3

4 Giusy A. Caprara[1*], Andrew A. Mecca[1,2*], Yanli Wang[3,4], Anthony J. Ricci[3,5], and
5 Anthony W. Peng[1]
6
7 **Abbreviated title:** Fast adaptation is not driven by calcium entry
8
9 **Author Affiliations:**
10 [1] Department of Physiology and Biophysics, University of Colorado Anschutz Medical
11 Campus, Aurora, CO 80045
12 [2] Neuroscience Graduate Program, University of Colorado Anschutz Medical Campus,
13 Aurora, CO 80045
14 [3] Department of Otolaryngology, Head and Neck Surgery, Stanford University School of
15 Medicine, Stanford, CA 94305
16 [4] Department of Mechanical Engineering and of Aeronautics and Astronautics, Stanford
17 University, Stanford, CA 94305
18 [5] Department of Molecular and Cellular Physiology, Stanford University School of
19 Medicine, Stanford, CA 94305
20 [*] Authors contributed equally
21
22 **Corresponding author:**
23 Anthony W. Peng (anthony.peng@ucdenver.edu)
24 Department of Physiology and Biophysics
25 University of Colorado, Anschutz Medical Campus
26 12800 E 19th Avenue
27 Rm 7127 MS 8307
28 Aurora, CO 80045
29
30

31 **Conflict of Interest:** All authors declare no competing financial interests.
32

Abstract:

Sound detection in auditory sensory hair cells depends on the deflection of the stereocilia hair bundle, which opens mechano-electric transduction (MET) channels. Adaptation is hypothesized to be a critical property of MET that contributes to the wide dynamic range and sharp frequency selectivity of the auditory system. Historically, adaptation was hypothesized to have multiple mechanisms, all of which require calcium entry through MET channels. Our recent work using a stiff probe to displace hair bundles showed that the fastest adaptation mechanism (fast adaptation) does not require calcium entry. Using a fluid-jet stimulus, others obtained data showing only a calcium-dependent fast adaptation response. Here, we identified the source of this discrepancy. Because the hair cell response to a hair bundle stimulus depends critically on the magnitude and time course of the hair bundle deflection, we developed a high-speed imaging technique to quantify this deflection. The fluid jet delivers a force stimulus, and step-like force stimuli lead to a complex time course of hair bundle displacement (mechanical creep), which affects the hair cell's macroscopic MET current response by masking the time course of the fast adaptation response. Modifying the fluid-jet stimulus to generate a step-like hair bundle displacement produced rapidly adapting currents that did not depend on membrane potential. This indicated that fast adaptation does not depend on calcium entry. We also confirmed the presence of a calcium-dependent slow adaptation process. These results confirm the existence of multiple adaptation processes: a fast adaptation that is not driven by calcium entry and a slower calcium-dependent process.

Significance Statement:

2

60   Mechanotransduction by sensory hair cells represents a key first step for the sound

61   sensing ability in vertebrates. The sharp frequency tuning and wide dynamic range of

62   sound sensation are hypothesized to require a mechanotransduction adaptation

63   mechanism. For decades, it had been accepted that all adaptation mechanisms require

64   calcium entry into hair cells. However, more recent work indicated that the apparent

65   calcium dependence of the fastest adaptation differs with the method of cochlear hair

66   cell stimulation. Here, we reconcile existing data and show that calcium entry does not

67   drive the fastest adaptation process, independent of the stimulation method.

68   **Introduction:**

69   Inner ear hair bundles comprise an array of graded length stereocilia that are

70   organized in a staircase manner. Positive hair bundle deflection increases tension in a

71   filamentous tip link that connects adjacent rows of stereocilia (1-3). Changes in tip-link

72   tension result in the gating of mechano-electric transduction (MET) ion channels.

73   MET adaptation is hypothesized to extend the dynamic range of the cell, control

74   the channel's operating point, and filter incoming stimuli (4-6). Adaptation is identified

75   by two phenomena: 1) a decay in current amplitude ("current decay") during a sustained

76   hair bundle displacement (5-8), and 2) a shift in the operating point (i.e., position along

77   the displacement axis) of the MET channel's current vs. displacement curve ("activation

78   curve"), without a change in the channel's sensitivity (i.e., the activation curve slope)

79   during a constant displacement step, hereafter called adaptation shift (5-7, 9). The

80   former is assayed using displacement steps and the latter is assayed using two-pulse

81   experiments, where an activation curve is generated before and after a sustained

82   displacement. In non-mammalian vertebrates, at least two adaptation processes have

83 been described, with different decay time constants, different extents, and different

84 calcium sensitivities (10-13). Slow adaptation has time constants of 10-100 ms and is

85 hypothesized to be a calcium-dependent modulation of tip-link tension via myosin motor

86 molecules controlling the position of the upper tip-link insertion site (14, 15). Fast

87 adaptation has a time constant of ~1 ms or less. Multiple potential mechanisms are

88 suggested for fast adaptation, all of which involve calcium entering through MET

89 channels and binding to an intracellular site that is either the channel itself or very close

90 to it (6, 14, 16-20).

91   Several experimental results from non-mammalian vertebrates support a model

92 in which calcium must enter the hair cell to affect both fast and slow adaptation: 1)

93 Current decay occurs at negative potentials where calcium entry occurs, but not at

94 positive potentials where calcium entry is inhibited (6, 21, 22). 2) Two-pulse experiments

95 demonstrate adaptation shifts at negative potentials that are modulated when using

96 different extracellular calcium concentrations (5-7). 3) The time constants of fast and

97 slow adaptation increase with increasing intracellular calcium buffering or decreasing

98 extracellular calcium concentrations (5, 6, 11, 20, 23). 4) The resting open probability of

99 MET channels, an indicator of the activation curve operating point, increases with lower

100 extracellular calcium concentration and upon depolarization (6, 11, 20, 24). These data

101 have been interpreted as supporting calcium-dependent adaptation mechanisms. Our

102 recent data from cochlear hair cells challenge this hypothesis for mammalian auditory

103 hair cells (12, 13, 25).

104   For *in vitro* MET experiments, stiff probes and fluid jets are the most commonly

105 used methods; they deliver step-like displacement or force stimuli to the hair bundle,

4

106   respectively. Stiff probes directly couple to stereocilia. In contrast, fluid jets eject

107   extracellular solution onto hair bundles from the tip of a pipette; the fluid velocity

108   produces a drag force stimulus on the hair bundle (26).

109   Our previous experiments with mammalian cochlear hair cells used stiff probe

110   stimuli (12, 13). Improvements to stiff probe technology produced step-like displacement

111   rise times as short as 11 μs (12), which provided finer temporal resolution of channel

112   activation and adaptation properties. With this technology, we found that fast adaptation

113   does not slow with depolarization or lower extracellular calcium and that adaptation

114   shifts are not affected by depolarization, suggesting that fast adaptation is not driven by

115   calcium entry (12). We performed multiple control experiments to rule out stimulus

116   artifacts (27) that might have been interpreted as fast adaptation (12). Furthermore, we

117   found that changes in the resting MET channel open probability induced by lowering

118   extracellular calcium or depolarization (experimental evidence 4) result from a lipid

119   modulation mechanism that is separate from fast adaptation and occurs with a time

120   constant of ~125 ms (13). Therefore, changes in MET channel resting open probabilty

121   alone cannot be used to support the calcium dependence of fast adaptation. These data

122   supported that fast adaptation was not driven by calcium entry.

123   In contrast, data acquired by other labs using fluid-jet stimulators with longer rise

124   times of ~500 μs suggest that fast adaptation is driven by calcium entry (28). The goal

125   of the present work is to reconcile these disparate findings.

126   We used a novel high-speed imaging system to quantify the magnitude and time

127   course of fluid-jet stimuli and the resulting hair bundle displacement. With step-like force

128   stimuli, the fast phase of the current decay was not observed at any potential. However,

129   with fluid-jet stimuli modified to produce step-like hair bundle displacements, similar to

130   what a stiff probe generates, we observed fast current decays; however, this did not

131   depend on the membrane potential. These results are consistent with our stiff probe

132   data and demonstrate that calcium entry does not drive the fast adaptation response.

133   **Results:**

134   *Mechanical creep in hair bundle displacement*

135   Stiff probe and fluid-jet stimulations are inherently different; the former delivers a

136   displacement and the latter a force. With the fluid jet, the resulting stereocilia

137   displacement elicited will vary depending on the mechanical properties of the stereocilia.

138   Thus, if the hair bundle dynamically changes its compliance, the resulting hair bundle

139   displacement will also change dynamically. Previous experiments measured hair bundle

140   movement using a photodiode system (14, 29, 30) or calibrated the fluid-jet driver

141   voltage to a hair bundle displacement (28, 31, 32). The photodiode method can only

142   image a portion of a hair bundle and assumes that the hair bundle moves as a unit.

143   Additionally, the photodiode method is experimentally difficult for two major reasons: 1)

144   the hair bundle needs to be precisely aligned with the photodiode, and 2) each

145   experiment requires a calibration to convert photodiode voltage to displacement.

146   Therefore, displacement measurements are often not done for all experiments. The

147   fluid-jet driver voltage calibration method assumes that hair bundle mechanical

148   properties (i.e., compliance) do not change for each stimulus paradigm or across

149   different cells and that the same force always results in the same hair bundle

150   displacement. However, mechanical properties are well-documented to change with

151   voltage and during stimulation (14, 33, 34), therefore invalidating this assumption.

152 To measure hair bundle displacement in every experiment, we developed a novel

153 method to quantify cochlear hair bundle displacement using high-speed imaging with

154 image analysis. Imaging at speeds up to 50,000 frames per second allowed tracking of

155 the motion of the whole hair bundle in all directions in the plane of imaging. This

156 technique is experimentally easier because: 1) only a one-time calibration of the size of

157 each pixel is required, and 2) no precise hair bundle alignment is required. To validate

158 our imaging technique, we compared the high-speed imaging technique with the

159 photodiode technique using a flexible glass fiber attached to a piezo-electric actuator.

160 We found similar results between the two methodologies (Fig. 1A). By allowing the

161 stimulated glass fiber to resonate, we demonstrated that the imaging approach had both

162 the speed and sensitivity necessary to track nanometer scale displacement on a sub-

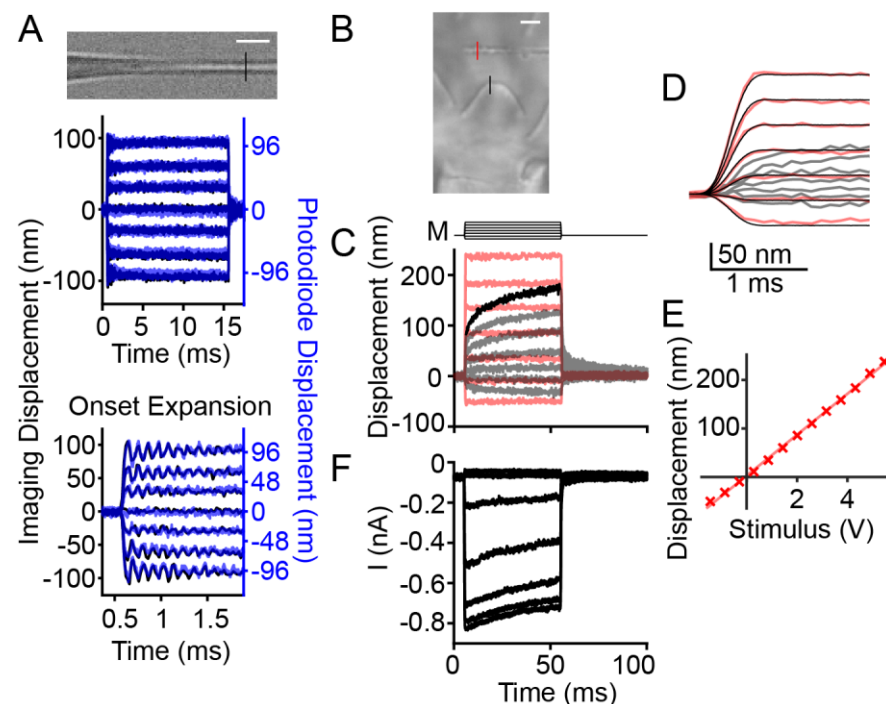163 millisecond timescale (Fig. 1A, bottom).

164

Fig. 1. Validation of imaging and stimulus techniques. (A) High-speed imaging of an
actuated flexible fiber at 50,000 frames per second (black traces) and the classical

7

167 photodiode technique (blue, semi-transparent) yielded similar results in fiber
168 displacement. An expansion of the onset of the fiber displacement showed an oscillation
169 of ~9 kHz with both techniques. (B) Image of a hair bundle is shown with a passive
170 flexible fiber in view to serve as a readout of the force applied by the fluid jet. Colored
171 lines indicate where motion was measured. (C) In a single stimulation protocol, we
172 monitored the fluid-jet force with the flexible fiber displacement (red), and we measured
173 hair bundle displacement (gray). The hair bundle has a continued movement in the
174 direction of the stimulation (i.e., mechanical creep, highlighted in one trace in black)
175 even when the force from the fluid jet was step-like. M indicates the fluid-jet stimulus
176 voltage waveform. (D) A time expansion of the onset of the fiber and hair bundle
177 displacements from C shows the short rise time of the force step. The stimulus waveform
178 (M, delayed and normalized) is overlaid in black to show that the stimulus voltage
179 waveform kinetics match the force output. (E) The fiber displacement plotted against the
180 stimulus voltage indicates linearity within the stimulus range used. (F) From the
181 experiment in panel C, the resulting MET current at -84 mV holding potential shows the
182 presence of slow current decay and the absence of fast current decay. Scale bars = 2
183 μm.

184

185   To confirm that the fluid-jet stimulator delivered a fast and step-like force, we used

186 the tip displacement of a non-actuated flexible fiber as a readout of the fluid-jet force

187 kinetics (Fig. 1B). The fiber moved as a step rising to a plateau in 0.5 ms, indicating that

188 the fluid-jet force (Fig. 1C,D, red) had the same onset kinetics as the stimulus voltage

189 (Fig. 1C, M traces; Fig. 1D, black traces). We also confirmed that force varied linearly

190 with driver voltage by plotting the fiber displacement against the stimulus voltage (Fig.

191 1E). Despite a step-like fiber displacement, the hair bundle in the same field of view

192 exhibited a mechanical creep (Fig. 1C, highlighted black trace), which is a continued

193 movement in the direction of the applied force. This creep indicates an increasing hair

194 bundle compliance as observed by others (14, 34-36). For the largest stimulation in 46

195 recorded cells, the creep was fit with a double exponential decay with time constants of

196 $\tau_1 = 1.8 \pm 0.8$ ms and $\tau_2 = 20.4 \pm 9.1$ ms with the slower time constant contributing 56.2

197 $\pm 6.9\%$ of the total creep. The recorded MET current elicited by fluid-jet force steps did

8

198   not show fast current decays (defined as exponential decay time constant < 5 ms) but

199   did show slow current decays (Fig. 1F). For step sizes eliciting ~50% of the maximum

200   current in the same 46 cells, current decays fit with a single exponential decay had τ =

201   26.5 ± 21.0 ms. These data indicate that step-like force stimuli exhibit hair bundle creep

202   and lack fast current decay.

203   We excluded the possibility that the observed creep was an artifact of underlying

204   epithelium movement by performing the same displacement analysis on features of the

205   epithelial surface below the hair bundle (Fig. S1). Changes in displacement from 0.5 ms

206   after stimulus onset to the end of the force step for the epithelial surface were much

207   smaller than the hair bundle creep for the same stimulus intensity (Fig. S1B). These

208   data suggest the creep was not an artifact of epithelial movement.

209   *Fast current decay present with overshoot stimuli only at negative potentials*

210   Unlike MET currents previously elicited with fluid-jet stimuli (28, 32), our MET

211   currents did not show a fast current decay (Fig. 1F). Upon detailed inspection of the data

212   from Corns et al. (2014), we found that they applied an underdamped step response,

213   which is characterized by an overshoot and ringing of their step stimulus. Both overshoot

214   and ringing are visible in their data with the carbon fiber. They used two carbon fibers to

215   characterize their force stimulus. The first fiber (8 μm diameter, see Corns et al. (2014)

216   Supplemental Fig. S2A) shows a step-like response with little to no evidence of an

217   underdamped response. However, this fiber has a rise time of ~2.5 ms, much longer

218   than the expected rise time of ~0.5 ms based on their stimulus voltage waveform. This

219   indicates that viscous drag on their long (>2 mm) carbon fibers filtered the force readout.

220   They also used a 10 μm diameter fiber with a shorter rise time of ~1.9 ms, indicating

9

221   less filtering and the ability to observe more of the stimulus kinetics. This fiber

222   displacement clearly shows an underdamped response (see Corns et al. (2014)

223   Supplemental Fig. S2B). If they had a faster readout of their force stimulus with a shorter

224   rise time of 0.5 ms (i.e., even less filtering of the response), they would likely observe

225   an even larger initial overshoot. The possibility that their stimulus driving circuit produced

226   ringing and that the fluid movement itself had ringing is further supported by the small

227   oscillations observed in their MET currents and hair bundle displacements whose

228   kinetics match the oscillations observed in their fiber displacement (see Corns et al.

229   (2014) Supplemental Fig. S3). We sought to test whether an underdamped stimulus

230   could account for the fast current decays observed by Corns et al. at negative potentials.

231   Based on the hair bundle displacement time course observed with our fluid-jet

232   stimuli, we predicted that an overshoot of a force step would result in an early plateau

233   of the hair bundle displacement. The fluid-jet stimulus used by Corns et al. (2014) led to

234   an early plateau in the hair bundle displacement (Fig. 2A arrow, black reproduced from

235   Corns et al. (2014)). We mimicked this key feature of the underdamped response to

236   achieve a similar early plateau in the hair bundle displacement (Fig. 2A, blue) by simply

237   using an overshoot stimulus with a single exponential decay back to steady state (Fig.

238   2B, arrow). Comparing our hair bundle displacement resulting from a step-like force to

239   that of Corns et al. (2014) also highlights the ringing in their hair bundle displacement

240   (Fig. 2A, magenta vs. black, arrowheads). Using an overshoot stimulation, we were able

241   to reproduce two key results observed by Corns et al. (2014) regarding fast adaptation.

242   1) Fast current decays, which look similar to current decays caused by fast adaptation,

243   were observed at negative potentials for positive displacements and upon returning from

10

244 a negative displacement (Fig. 2B, arrowheads). 2) Both of these fast current decays

245 were absent at positive potentials (Fig. 2B). When returning to a step-like force stimulus

246 in the same cell, we observed our typical responses where no fast current decays were

247 present (Fig. 2C). Interestingly, these results show that a small difference in the hair

248 bundle displacement (Fig 2A, blue vs. magenta) led to a large difference in the MET

249 current (Fig. 2B,C), which reinforces the hair bundle's sensitivity to small displacement

250 changes. These results indicate that the fast current decays observed by Corns et al.

251 (2014) could be an artifact of an underdamped stimulus and not a manifestation of fast
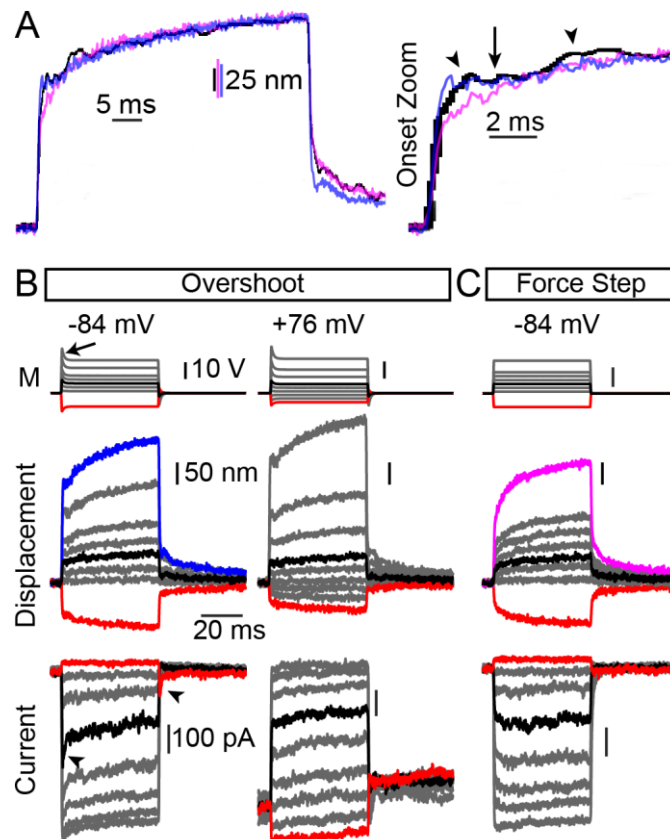
252 adaptation.

253

255 **Fig. 2.** Overshoot stimuli can account for fast current decays observed by Corns et al.
256 (2014). (A) To mimic the displacement responses of Corns et al. (2014) (black traces,

257 reproduced from Corns et al. (2014)), we modified our step-like force stimulus (resulting
258 displacement in magenta) to achieve an early plateau (arrow in onset zoom) in the
259 displacement response using an overshoot stimulus (resulting displacement in blue). An
260 expansion of the onset is shown to the right with the early plateau (arrow) and the
261 oscillations (arrowheads) in the black trace indicated. (B) The stimulus waveform,
262 resulting hair bundle displacements, and the recorded currents are plotted. Using 1 mM
263 intracellular BAPTA buffer, overshoot stimuli resulted in current decays that appear like
264 fast adaptation (arrowheads). In the same cell, the fast current decays were absent at
265 positive potentials with overshoot stimuli. (C) When removing the overshoot and using
266 a step-like force stimulation in the same cell, no fast current decays are evident at
267 negative potentials. No averaging of stimulations was used, and current traces were 5
268 point smoothed using MATLAB's smooth function; displacement traces were averaged
269 over 14 lines around the apex of the hair bundle.

270

271 *Adaptation shifts indicate an adaptation mechanism that does not require calcium entry*

272 Measuring adaptation shifts in response to a constant adapting step with a two-

273 pulse protocol assesses adaptation (5, 12). Our experiments with a stiff probe in

274 cochlear hair cells using two-pulse protocols found that the adaptation shifts for 5 ms

275 sustained displacements were the same at negative and positive potentials (12), while

276 others using a fluid jet found that adaptation shifts for 20 ms of sustained force stimuli

277 were present at negative potentials but absent at positive potentials (28). The fluid-jet

278 data did not have corresponding hair bundle displacement with each fluid-jet

279 experimental paradigm; therefore, the data did not account for the mechanical creep

280 (see Corns et al. (2014) Methods, last paragraph). Although the results are presented

281 as current vs. displacement plots, they represent current vs. stimulus voltage plots. We

282 performed these experiments while measuring hair bundle displacement using the high-

283 speed imaging system, allowing us to simultaneously generate current vs. stimulus

284 voltage and current vs. displacement plots. We used a three-pulse protocol where we

285 assayed the adaptation shifts at 10 ms and 50 ms after the start of a sustained force

12

286   step with 5 ms test pulses to generate the activation curve (Fig. 3A, M traces). We

287   recapitulated the findings of Corns et al. (2014) with current vs. stimulus voltage plots

288   (Fig. 3A, B), where a shift occurred at negative but not positive potentials. Additionally,

289   current decay was observed at negative, but abolished at positive potentials (Fig. 3A,

290   arrowheads). The current decay at negative potentials during the first 10 ms of the

291   sustained force stimulus was fit with a single exponential decay $\tau = 14.0 \pm 1.5$ ms (n =

292   6), a time scale consistent with slow adaptation. These results could be interpreted as

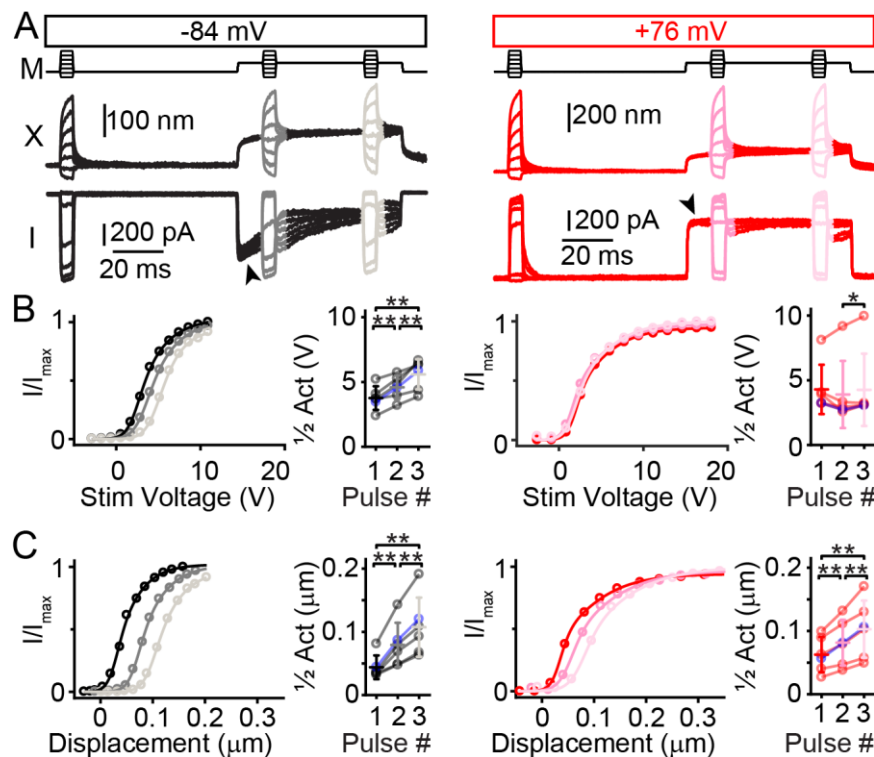293   only calcium-dependent adaptation mechanisms.

294

295   **Fig. 3.** Three-pulse experiments to assay adaptation shifts using a fluid-jet stimulus and
296   0.1 mM BAPTA intracellular solution. (A) Voltage commands for the fluid jet in a three-
297   pulse protocol are shown (M) at -84 mV (black) and at +76 mV (red) holding potentials
298   with measured hair bundle displacements (X) and currents (I). Arrowheads indicate
299   current decay at negative, but not positive potentials. (B) Analyzing data with the
300   stimulus voltage showed activation curve shifts at negative potentials, but not positive
301   potentials. Summary data of half activation points for each stimulus pulse show positive
302   adaptation shifts at negative (n=6, pulse 1-2 p=0.0029, 2-3 p=0.0066, and 1-3
303   p=0.0039), but not positive potentials (n=6, pulse 1-2 p= p=0.28, 2-3 p=0.034, and 1-3

304 *p*=0.94). Blue data points are from traces in A. (C) Analyzing data with measured hair
305 bundle displacement indicates adaptation shifts at both negative (n=6, pulse 1-2
306 *p*=0.0050, 2-3 *p*=0.0021, and 1-3 *p*=0.0033), and positive potentials (n=6, pulse 1-2
307 *p*=0.0045, 2-3 *p*=0.0042, and 1-3 *p*=0.0039).

308

309   In contrast, plotting the same currents against measured hair bundle

310 displacement demonstrated adaptation shifts at both negative and positive potentials

311 (Fig. 3C). These data suggested that adaptation shifts and current decays were

312 decoupled when using sustained force stimuli because adaptation shifts occurred in the

313 absence of current decays at positive potentials. Unlike our data with stiff probes (12),

314 adaptation shifts with the fluid jet were significantly larger at negative potentials (35 ± 18

315 nm at 10 ms and 63 ± 30 nm at 50 ms, n = 6) than at positive potentials (19 ± 9 nm and

316 40 ± 19 nm at 50 ms, n = 6; *p*=0.035 at 10 ms and *p*=0.023 at 50 ms). These data could

317 be interpreted in two ways with regard to the calcium dependence of adaptation. One

318 interpretation is that since adaptation shifts occurred at positive potentials, there is an

319 adaptation process that is not driven by calcium entry. That the adaptation shifts were

320 larger at negative potentials as compared to positive potentials would indicate that there

321 is a second calcium-dependent adaptation process; this could be the slow adaptation

322 studied by others with a time course of ~10 ms (5, 21). An alternative interpretation is

323 that all the adaptation observed at positive potentials is residual calcium-dependent slow

324 adaptation. The motor model of slow adaptation does not preclude slow adaptation from

325 occurring at positive potentials, since only the rate of adaptation is modulated by calcium

326 entry (15). Although this is theoretically possible for the motor model, it has not been

327 observed in non-mammalian hair cells, as no slow current decays resulting from

328 displacement steps are observed during depolarization (6, 20, 21, 24). Here, the

329 adaptation shift at positive potentials after 10 ms was 47.5% of the shift after 50 ms. If

330   all of the adaptation shift was due to slow adaptation, then based on the single

331   exponential decay equation, the time constant of the slow adaptation at positive

332   potentials would need to be 16.7 ms (see methods for calculation), similar to the slow

333   adaptation time constant at negative potentials of 14 ms. Since the time constants would

334   be similar at negative and positive potentials, this would not fit with the motor model of

335   slow adaptation, which predicts that the rate of adaptation at positive potentials is much

336   slower than at negative potentials (15, 24). Therefore, the more likely interpretation is

337   the existence of two adaptation mechanisms that differ in calcium dependence: a fast

338   adaptation that does not require calcium entry and a slow adaptation that depends on

339   calcium.

Step-like displacement stimulations with the fluid jet unmask fast current decays

341   To further support the existence of two adaptation mechanisms with different

342   calcium requirements, we tested if fast current decays could be observed at positive

343   potentials using step-like displacement stimuli. We wondered if the fast current decays

344   were masked by the hair bundle creep (Fig. 1C), where continued hair bundle movement

345   counteracted the current decay and would be responsible for the lack of visible fast

346   current decays with step-like force stimuli. To test this, we designed a circuit to modify

347   the fluid-jet voltage waveform to create a step-like displacement of the hair bundle (Fig.

348   4A). To limit the contribution of calcium-dependent adaptation mechanisms, we used a

349   high intracellular calcium buffer (10 mM BAPTA) in these experiments. We applied both

350   step-like force and step-like displacement stimuli on the same cell for these experiments.

351   Consistent with Figs. 1F and 2C, fast current decays were absent at both negative and

352   positive potentials with step-like *force* stimuli (Fig. 4A). In the same cell with step-like

353 *displacement* stimuli, fast current decays were present at both negative and positive

354 potentials (Fig. 4A, arrowheads). For displacement steps eliciting ~50% maximum

355 current, the fast current decay was similar at negative and positive potentials: at negative

356 potentials it had a time constant of 1.6 ± 1.2 ms and contributed 34 ± 14% (n = 7) of the

357 total extent of adaptation, and at positive potentials it had a time constant of 1.8 ± 1.4

358 ms and contributed 29 ± 17% (n = 6) of the total extent of adaptation (p = 0.99 and p =

359 0.32, respectively; paired Student's t-test between negative and positive potentials). The

360 slow current decay, on the other hand, was faster at negative potentials (14 ± 3 ms; n =

361 7) than at positive potentials (59 ± 41 ms; n = 6; p = 0.053, paired Student's t-test).

362 These data further support that all adaptation at positive potentials cannot be accounted

363 for by residual slow adaptation, since a measured time constant of 1.8 ± 1.4 ms (n = 6)

364 (Fig. 4A) is too fast for slow adaptation. The fast current decays at both negative and

365 positive potentials (Fig. 4A, arrowheads) supported the conclusion that fast adaptation

366 was not driven by calcium entry.

367   With step-like displacements, the amount of adaptation increased significantly. A

368 fast time constant of 1.6 ± 1.2 ms and a slow time constant of 14 ± 3 ms suggests that

369 the total adaptation measured at 5 ms is predominately fast adaptation. We used the

370 difference in total adaptation between the time points of 50 ms and 5 ms to quantify slow

371 adaptation. The amount of total adaptation observed as current decays increased with

372 step-like displacements at 50 ms (Fig. 4B), 5 ms (Fig. 4C), and between 5 and 50 ms

373 (Fig. 4D) for both negative and positive potentials with no significant difference between

374 the two potentials (p = 0.61, 0.16, and 0.56, respectively). The time to peak current

375 decreased with displacement stimuli (Fig. 4E), indicating that the current onset is slowed

376   with force stimuli. Across negative and positive potentials, step-like displacements

377   increased the adaptation at 5 ms by 17 ± 8% and the adaptation between 5 and 50 ms

378   by 12 ± 8%, indicating that the step-like displacements led to a greater enhancement of

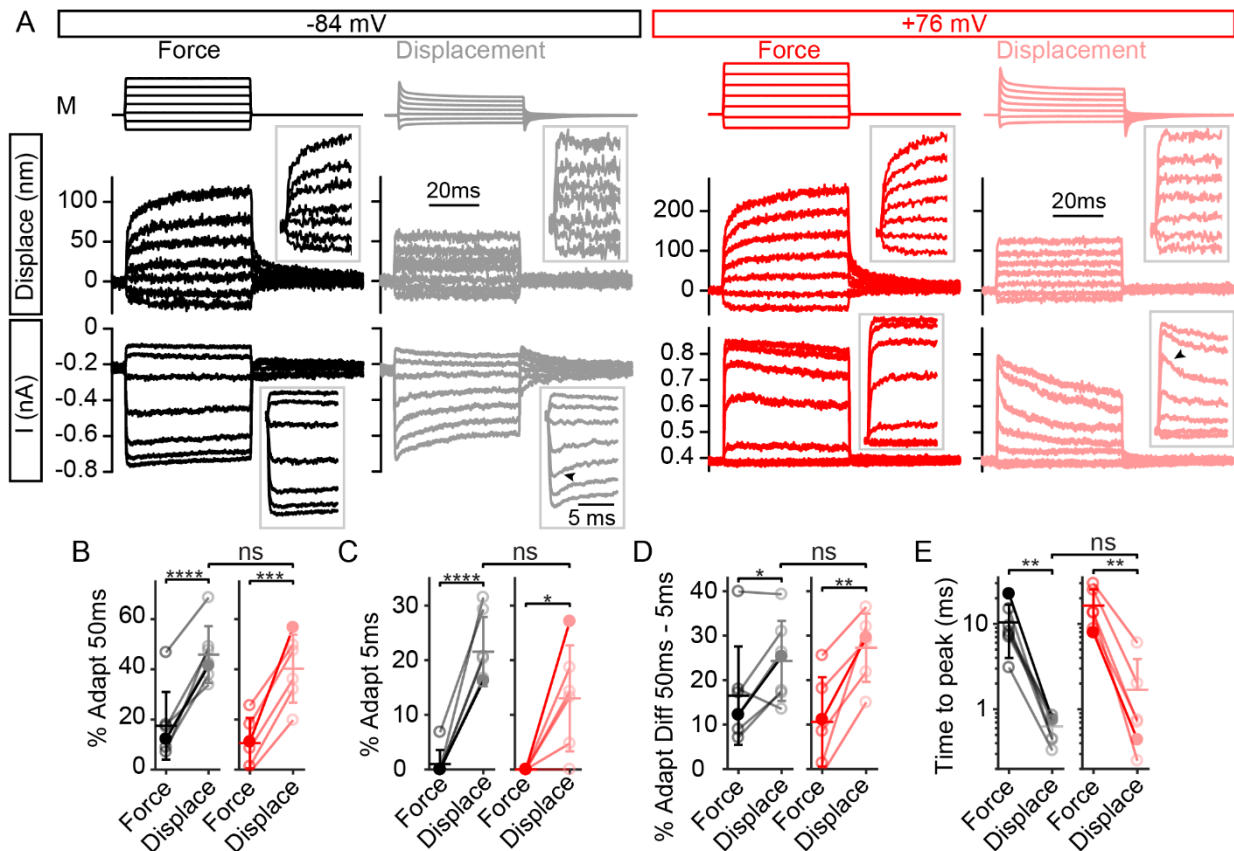379   fast current decays.

380

381

Fig. 4. Step-like hair bundle displacement with the fluid jet unmasked fast adaptation in the current response. (A) At negative potentials, step-like force stimulation (black) resulted in hair bundle creep with no visible fast adaptation in the current. With step-like displacement stimuli (gray), fast adaptation in the current was visible (inset, arrowhead). Similarly, at positive potentials, no fast adaptation was observed with step-like force stimulation (red), but fast adaptation was unmasked with step-like displacements (pink, arrowhead). Displacement was measured in the vertical direction near the middle of the hair bundle at the same location for each stimulus paradigm. Inset traces are expanded to fill the space to better see the onset of the stimuli. (B) Summary of the amount of total adaptation at the 50 ms timepoint between the step-like force and step-like displacement stimulation showed a significant difference between force and displacement stimuli

393 (n=7, -84 mV, p=0.000090; n=6, +76 mV, p=0.00038). (C) The amount of adaptation at

394 5 ms would have almost all fast adaptation complete and a small contribution from the

395 slow adaptation process. Adaptation at 5 ms also showed a significant increase

396 indicating the presence of fast adaptation (n=7, -84 mV, p=0.000056; n=6, +76 mV,

397 p=0.022). (D) The difference in adaptation between the 50 ms and 5 ms time points

398 would be almost completely composed of slow adaptation. This had a significant

399 increase at +76 mV with step-like displacements (n=7, -84 mV, p=0.032; n=6, +76 mV,

400 p=0.0028). For all adaptation quantifications, step-like displacement responses were not

401 significantly different between negative and positive potentials. (E) Using step-like

402 displacements shortens the time to peak current at both negative and positive potentials

403 (n = 7, -84 mV, p=0.0067; n = 6, +76 mV, p=0.0038).

404

405 **Discussion:**

406   Our data with the fluid jet are consistent with our previous work using a stiff probe,

407 which demonstrate that fast adaptation is not driven by calcium entry (12). Accounting

408 for hair bundle displacement in three-pulse experiments with fluid-jet stimuli revealed

409 adaptation shifts at positive potentials. Step-like force and displacement stimuli result in

410 different MET current responses. Step-like *force* stimuli results in a mechanical creep

411 with two time constants, which mask the fast current decay associated with fast

412 adaptation. Step-like *displacement* stimuli result in fast current decays at both negative

413 and positive potentials, indicating that calcium entry does not drive fast adaptation.

414 *Fast adaptation is not driven by calcium entry*

415   After we proposed that calcium entry does not drive fast adaptation (12), others

416 suggested that the results we observed with the stiff probe were an artifact of the

417 stimulus (28). However, we found that PIP_2 depletion resulted in a loss of fast adaptation

418 with stiff probe stimuli (25), indicating that fast adaptation with the stiff probe data is not

419 a stimulus artifact.

420   The resting open probability increases with low extracellular calcium or

421 depolarization, and adaptation regulates open probability, which has been taken to

422   argue that lower extracellular calcium and depolarization regulate adaptation. However,

423   mammalian cochlear hair cells can regulate resting open probability by modulating the

424   lipid membrane, independent of fast adaptation (13). Therefore, direct assays are

425   required to test whether calcium entry drives fast adaptation.

426   We now also demonstrate that data from Corns et al. (2014) using the fluid jet to

427   support calcium-driven fast adaptation can have a different interpretation. Importantly,

428   force and displacement stimuli are not the same. When assaying adaptation with a fluid

429   jet, hair bundle displacement must be quantified because of hair bundle creep. When

430   measuring hair bundle displacement, we observe adaptation that is not driven by

431   calcium entry in three-pulse experiments and that cannot be accounted for by residual

432   slow adaptation (Fig. 3).

433   We also hypothesize that Corns et al. used an underdamped stimulus that

434   created a time-dependent decrease in current amplitude that appeared to be fast

435   adaptation. We simulated their underdamped stimulus by using an overshoot stimulus

436   (Fig. 2). Under these conditions, fast time-dependent current decays were present at

437   negative but not positive potentials, as with their observation. This result can be mis-

438   interpreted as fast adaptation driven by calcium, when in fact it is due to a stimulus

439   artifact.

440   Interestingly, an overshoot stimulus can result in current decays at negative, but

441   not positive potentials (Fig. 2B). Initially, we expected the overshoot artifact to cause a

442   similar response at negative and positive potentials. The different responses indicate

443   that there are some properties that are modulated by voltage. Upon further investigation,

444   this result may be due to differences in current rise time. At positive potentials, the

19

445 current rise time is longer (Fig. 4E). When the overshoot artifact occurs during the longer

446 current rise, it can result in shortening the current rise time and can mask the current

447 decay (see supplemental text), similar to early plateau in the hair bundle displacement

448 using the same stimulus (Fig. 2A onset zoom). Another factor contributing to the lack of

449 fast current decays at positive potentials with an overshoot stimulus is the presence of

450 the slower hair bundle creep component. The slow creep of the hair bundle causes

451 further opening of MET channels, which can reverse any fast current decay and make

452 the current appear to have a stimulus anomaly, rather than being interpreted as a current

453 decay. For example, in Kros et al. (2002), Fig. 2B shows hints of a fast current decay at

454 positive potentials, but the continued current rise due to the slower creep makes the

455 current decay appear like a small notch and not the result of a fast adaptation

456 mechanism.

457   The most convincing result is the appearance of fast current decays with a fluid-

458 jet stimulus regardless of membrane potential when the driving voltage is modified to

459 achieve a step-like displacement. The step-like displacement most closely mimics the

460 typical step stimuli of a stiff probe. The differences between stimulation methods is

461 complex, such that we do not expect that providing a displacement stimulus with the

462 fluid jet would result in the same exact response we observe with the stiff probe. Notably,

463 the extent of fast adaptation appears greater with the stiff probe (12) than with the fluid

464 jet (Fig. 4A). This discrepancy may be caused by multiple differences in the

465 characteristics of the stimulation methods. Lengthening the stimulation rise time

466 increases the fast adaptation time constant and reduces its extent (10, 27), so

467 differences in stimulus rise times between stimulation methods are likely a major

20

468   contributing factor. Other contributing factors are the differences in mechanical loading

469   of the hair bundle and pulling of shorter rows of stereocilia due to taller rows moving

470   versus pushing shorter row stereocilia directly. It is unlikely that any one of these is

471   solely responsible for the discrepancy in the adaptation extent. Although the exact

472   responses differ, the basic result remains valid, i.e., that fast adaptation exists at positive

473   potentials and is not driven by calcium entry.

474   We discuss the Corns et al. (2014) paper because it has the most comprehensive

475   data set supporting calcium-driven fast adaptation; however, other papers have also

476   shown adaptation at negative, but not positive potentials. Indzhykulian et al. used a stiff

477   probe and found that fast adaptation was more prominent at negative than positive

478   potentials (37). These authors assumed the absence of fast adaptation at positive

479   potentials; therefore, they positioned the probe to minimize fast adaptation as a way of

480   avoiding what they assumed was a stimulus artifact (see their results section

481   *Regeneration of MET Occurs in Two Distinct Steps*). Fast adaptation can be saturated

482   even at negative potentials (see Peng et al. (2013), Supplemental Fig. S1). An

483   alternative explanation to their data is that depolarization modulates the saturation point

484   of fast adaptation and that the difference they observed was a voltage-dependent

485   difference between a saturated and unsaturated fast adaptation. Though the correct

486   positioning of a stiff probe is debatable, the fluid jet does not have the same positioning

487   problems, and we still observe fast current decays at positive potentials using a step-

488   like displacement stimuli with the fluid jet (Fig. 4A).

489   In another paper, Beurg et al. claimed adaptation shifts at negative, but not

490   positive potentials when measuring displacement (31). There are a few concerns with

21

491   these data and their interpretation. First, the displacement traces do not exhibit the hair

492   bundle creep that we, the authors themselves in another study, and others have

493   observed (Fig. 1C) (28, 33-36, 38). Second, the test pulses after the sustained stimulus

494   do not cover the full range of the activation curve, where not enough negative steps are

495   delivered to determine the minimum MET current after the sustained stimulus. Third,

496   their data show a small adaptation shift at positive potentials. More information about

497   their stimulus and new data with more stimulation steps are needed to resolve this

498   potential discrepancy.

499   When discussing adaptation, all mechanisms are often considered together, but

500   there are potentially at least 3 mechanisms: fast adaptation, slow adaptation, and lipid

501   modulation. The latter 2 mechanisms are calcium-dependent. Two recent reports claim

502   that in Tmc1 mutant cells (*Beethoven)* with altered calcium permeability, steady-state

503   changes in the activation curve support calcium-dependent adaptation (31, 32).

504   However, neither study directly tests for the calcium dependence of fast adaptation.

505   Corns et al. (2016) performed step stimuli with their fluid jet, which can directly assay

506   fast adaptation (see their Fig. 4-6), but they are likely using an underdamped stimulus.

507   Even so, the data presented have no noticeable effect on fast adaptation. If fast

508   adaptation were driven by calcium entry, then the lowered calcium permeability in the

509   mutant cells would be expected to increase the fast adaptation time constant and/or

510   decrease the extent; however, neither of these occur, which supports that calcium entry

511   does not drive fast adaptation. When interpreting data about the calcium dependence

512   of adaptation, it is important to separate the different mechanisms (fast, slow, and lipid

513   regulation) and to assay each separately on their respective time scales.

22

514   *Mechanisms of adaptation*

515   Adaptation is hypothesized to contribute to the hair cell's dynamic range and

516   frequency selectivity (4, 6); therefore, determining its mechanism is important. Knowing

517   that fast adaptation is not driven by calcium entry is an important step because it narrows

518   the list of possible mechanisms. The manifestation of adaptation differs depending on

519   the mode of stimulation; current decays are observed for displacement steps and hair

520   bundle creep for force steps. This suggests that the hair bundle creep could be a

521   manifestation of fast adaptation (34). One attractive mechanistic model of the creep is

522   viscoelasticity, which is modeled with a spring and dashpot and could indicate a

523   viscoelastic process underlying fast adaptation (14, 39). No direct evidence yet exists in

524   support of a unique mechanism for fast adaptation.

525   Our data also confirm the presence of a calcium-dependent adaptation

526   mechanism with time constants of ~10 ms. The motor model of slow adaptation

527   proposes that myosin motors dynamically adjust the position of the upper tip-link

528   insertion site to modulate the force transferred to the MET channel depending on the

529   local calcium levels. This model requires a calcium source, namely MET channels, to

530   be localized near the upper insertion site. In mammalian auditory hair cells, the MET

531   channels were localized to the tips of the shorter stereocilia and not near the upper

532   insertion site (40). The channel localization along with the fact that mammalian hair

533   bundles only consist of three rows of stereocilia eliminated the possibility of a direct

534   calcium source modulating myosin motors at the upper tip-link insertion site, therefore

535   questioning the validity of the motor model of slow adaptation (12). Thus, the slow

536   adaptation mechanism may not involve the slipping of myosin motors along the sides of

23

537 stereocilia. The MET system would still require a tip-link tensioning mechanism in order

538 to have high sensitivity, and myosin motors are the likely candidates for the tensioning

539 mechanism. Myosin motors can still be required to climb up stereocilia to generate

540 tension, but do not regulate the tension directly due to calcium entering through MET

541 channels.

542   The results in this study confirm that fast adaptation is not driven by calcium entry

543 but that slow adaptation is, reconciling previously conflicting data. The mechanisms of

544 fast and slow adaptation require new molecular models of their function.

545 **Materials and Methods**:

546 *Preparation and recordings*: Animals were euthanized by decapitation using methods

547 approved by the University of Colorado IACUC. Organs of Corti were dissected from

548 postnatal day (P) 6-10 Sprague-Dawley rats (a large majority of experiments used P7-

549 P8) of either sex. The tectorial membrane was peeled off, and the tissue was placed in

550 recording chambers as previously described (40). Tissue was viewed using a 60x or

551 100x (1.0 NA, Olympus) water immersion objective with a Phantom Miro 320s (Vison

552 Research) camera on a SliceScope (Scientifica) illuminated with a TLED+ 525 nm LED

553 (Sutter Instruments). Tissue was dissected and perfused with extracellular solution

554 containing (in mM): 140 NaCl, 2 KCl, 2 $CaCl_2$, 2 $MgCl_2$, 10 HEPES, 2 creatine

555 monohydrate, 2 Na-pyruvate, 2 ascorbic acid, 6 dextrose, pH=7.4, and 300-310 mOsm.

556 In addition, an apical perfusion, using pipettes with tip sizes of 150-300 μm, provided

557 local perfusion to the hair bundles.

558 *Electrophysiological recordings:* Whole-cell patch-clamp was achieved on the first or

559 second row outer hair cells (OHCs) from the middle to apical cochlear turns using an

24

560   Axon 200B amplifier (Molecular Devices) with thick-walled borosilicate patch pipettes

561   (2-6 MΩ) filled with an intracellular solution containing (in mM): 125 CsCl, 3.5 MgCl$_2$, 5

562   ATP, 5 creatine phosphate, 10 HEPES, 1 cesium BAPTA, 3 ascorbic acid, pH=7.2, and

563   280-290 mOsm. For the 0.1 mM and 10 mM BAPTA internal solution, the BAPTA

564   concentration was adjusted accordingly, and CsCl concentrations were adjusted to

565   reach 280-290 mOsm. Experiments were performed at 18-22°C. Whole cell currents

566   were filtered at 10 kHz and sampled at 0.05-1 MHz using USB-6356 (National

567   Instruments) controlled by jClamp (SciSoft Company). Voltages were corrected offline

568   for liquid junction potentials. All experiments used -84 mV holding potential unless

569   otherwise noted. An apical perfusion pipette with extracellular solution was used during

570   patching of hair cells. Only cells with initially < 100 pA of leak were kept for data analysis,

571   except when using 10 mM intracellular BAPTA where < 200 pA was used. Cells also

572   required > 550 pA of initial peak MET current. During a prolonged depolarization, the

573   cell changes resting open probability (12, 13). To have a stable baseline during the

574   positive potential protocols, the cell was depolarized for >10 s to allow the open

575   probability to settle. None of the data presented have had the baseline current zeroed.

576   *Hair bundle stimulation and motion recording*: Hair bundles are stimulated with a custom

577   3D printed fluid jet driven by a piezo electric disc bender (27 mm 4.6 kHz; Murata

578   Electronics 7BB-27-4L0). Thin wall borosilicate pipettes were pulled to tip diameters of

579   5-20 micrometers, filled with extracellular solution, and mounted in the fluid-jet

580   stimulator. The piezo disc bender was driven by waveforms generated using jClamp,

581   and the signals were filtered using an 8-pole Bessel filter (L8L 90PF, Frequency Devices

582   Inc.) at 1 kHz and variably attenuated (PA5, Tucker Davis) before being sent to a high

583   voltage/high current amplifier (Crawford amplifier) to drive the piezo disc bender. During

584   stimulations, videos were taken of the hair bundle motion with high speed imaging at

585   10,000 frames per second using the Phantom Miro 320s at 128 x 128 pixels with a 100

586   nm effective pixel size. Videos were saved for each stimulation and analyzed offline.

587   Four stimulus presentations were averaged together at each stimulus level unless

588   otherwise stated. In some experiments, a short flexible fiber (long fibers have too much

589   viscous drag) was used to monitor the force of the fluid-jet stimulation. Some fibers were

590   dipped in an oil-based ink to increase fiber contrast. Photodiode measurements were

591   done using a custom-built dual photodiode (SPOT-3D, OSI Optoelectronics) with a

592   custom built onboard differential trans-impedance amplifier (12).

593   For achieving a step-like hair bundle stimulation with the fluid jet, the voltage step

594   response was fed into a custom-built circuit that mimicked a supercharging circuit with

595   an exponential decay (41). We required two exponential decays to achieve a step-like

596   bundle displacement, so two supercharging circuits were used in series where variable

597   resistors allowed modification of the decay magnitude and time constant to match the

598   observed hair bundle creep. The decay time constants were manually adjusted for each

599   cell to yield a step-like displacement of the hair bundle. These parameters were then

600   fixed for both negative and positive potential protocols for that cell and protocols were

601   taken one after another.

602   *Hair bundle motion analysis*: Custom MATLAB (MathWorks) scripts were used for

603   extraction and analysis of the hair bundle motion. Movie frames were imported into

604   MATLAB and the position of the hair bundle was extracted using a Gaussian fit to a

605   band-pass filtered image (42) for a given vertical row of pixels in the image to yield sub-

606   pixel resolution. For most cells, the vertical displacement of the hair bundle near its

607   center was taken as the displacement of the hair bundle.

608   *Data analysis:* IX plots used the displacement data from the high-speed imaging taking

609   the displacement values at when the peak current occurred for 50 ms step traces. For

610   three-pulse protocols, displacement and current were taken 1 ms after stimulus onset,

611   because the steps were short (5 ms) and peak currents were not always reached during

612   this time period. Normalized currents (I/I_{max}) were generated by subtracting the leak

613   current defined as the smallest remaining current during the negative steps and

614   normalizing to the peak current. IX plots were automatically fit using MATLAB with a

615   double Boltzmann equation:

616
$$y = \frac{I_{max}}{1+e^{Z_2(x_0-x)}(1+e^{Z_1(x_0-x)})} \qquad (2)$$

617   Where Z_1 and Z_2 were the slope factors and x_0 was the set point.

618   For mechanical stimulus steps, a double exponential decay equation was

619   automatically fit in MATLAB using steps that elicited ~50% maximum current:

620
$$y = y_0 + A_1 e^{-(x-x_0)/\tau_1} + A_2 e^{-(x-x_0)/\tau_2} \qquad (3)$$

621   Where τ_1 and τ_2 were the decay constants and A_1 and A_2 were the respective

622   amplitudes. $A_1/(A_1+A_2)$ is the contribution of fast adaptation and $A_2/(A_1+A_2)$ is the

623   contribution of slow adaptation to the total extent of adaptation. The displacement of the

624   hair bundle was also fit with the same equation starting at the timepoint after the force

625   of the stimulus plateaued, which was 0.5 ms after stimulus onset. Percent adaptation

626   was calculated as $(1 - I_{steady\ state}/I_{peak})$ * 100 for the step that was closest to 50%

627   maximum current.

27

628   The time constant calculation based on the adaptation shifts at 10 ms and 50 ms

629   was calculated using the single exponential decay equation. The amount of adaptation

630   occurring at 10 ms is expressed as $A_1 \left(1 - e^{\frac{-10}{\tau}} \right)$ and the amount of adaptation at 50 ms

631   is expressed as $A_1 \left(1 - e^{\frac{-50}{\tau}} \right)$ with τ expressed in ms. The ratio of these is equal to 0.475

632   based on the measurements. This can be rearranged to:

633
$$A_1 \left(1 - e^{\frac{-10}{\tau}} \right) - 0.475 * A_1 \left(1 - e^{-\frac{50}{tau}} \right) = 0$$

634   Graphing the left side of the equation and looking for the zero crossings indicates only

635   one zero crossing at τ = 16.7 ms.

636   All n's presented were biological replicates of individual cells, where only one cell

637   was used per animal. Each data point was the average of 4 presentations of the same

638   stimulus intensity (technical replicates), unless otherwise noted.

639   Data were analyzed using jClamp, MATLAB (MathWorks), and Excel (Microsoft).

640   Graphs were created using MATLAB and Adobe Illustrator. The mechanosensitive

641   current/maximum mechanosensitive current was used as P_{open}, where we assume an

642   observable P_{open} of 100%. The maximum MET current was the difference between the

643   current values elicited from the maximal negative and maximal positive stimulation.

644   Statistical analysis used Student's two-tailed t-tests from MATLAB or Excel

645   (Microsoft) unless otherwise stated. Paired tests were used when comparing across

646   data points in the same cell, and unpaired-unequal variance tests were used to compare

647   data across cell populations. Significance (*p*-values) were as follows: * $p<0.05$, **

648    $p<0.01$, *** $p<0.001$, **** $p<0.0001$. Data were presented as mean ± standard deviation

649   unless otherwise noted.

650

References:

1. Kazmierczak P*, et al.* (2007) Cadherin 23 and protocadherin 15 interact to form tip-link filaments in sensory hair cells. *Nature* 449(7158):87-91.
2. Ahmed ZM*, et al.* (2006) The tip-link antigen, a protein associated with the transduction complex of sensory hair cells, is protocadherin-15. *J Neurosci* 26(26):7022-7034.
3. Kachar B, Parakkal M, Kurc M, Zhao Y, & Gillespie PG (2000) High-resolution structure of hair-cell tip links. *Proc Natl Acad Sci U S A* 97(24):13336-13341.
4. Ricci AJ, Kennedy HJ, Crawford AC, & Fettiplace R (2005) The transduction channel filter in auditory hair cells. *J Neurosci* 25(34):7831-7839.
5. Eatock RA, Corey DP, & Hudspeth AJ (1987) Adaptation of mechanoelectrical transduction in hair cells of the bullfrog's sacculus. *J Neurosci* 7(9):2821-2836.
6. Crawford AC, Evans MG, & Fettiplace R (1989) Activation and adaptation of transducer currents in turtle hair cells. *J Physiol (Lond)* 419:405-434.
7. Corey DP & Hudspeth AJ (1983) Analysis of the microphonic potential of the bullfrog's sacculus. *J Neurosci* 3(5):942-961.
8. Eatock RA (2000) Adaptation in hair cells. *Annu Rev Neurosci* 23:285-314.
9. Fettiplace R & Kim KX (2014) The Physiology of Mechanoelectrical Transduction Channels in Hearing. *Physiological reviews* 94(3):951-986.
10. Wu Y-C, Ricci AJ, & Fettiplace R (1999) Two Components of Transducer Adaptation in Auditory Hair Cells. *J Neurophysiol* 82(5):2171-2181.
11. Ricci AJ, Wu YC, & Fettiplace R (1998) The endogenous calcium buffer and the time course of transducer adaptation in auditory hair cells. *J Neurosci* 18(20):8261-8277.
12. Peng AW, Effertz T, & Ricci AJ (2013) Adaptation of mammalian auditory hair cell mechanotransduction is independent of calcium entry. *Neuron* 80(4):960-972.
13. Peng AW, Gnanasambandam R, Sachs F, & Ricci AJ (2016) Adaptation Independent Modulation of Auditory Hair Cell Mechanotransduction Channel Open Probability Implicates a Role for the Lipid Bilayer. *J Neurosci* 36(10):2945-2956.
14. Howard J & Hudspeth AJ (1987) Mechanical relaxation of the hair bundle mediates adaptation in mechanoelectrical transduction by the bullfrog's saccular hair cell. *Proc Natl Acad Sci U S A* 84(9):3064-3068.
15. Gillespie PG & Cyr JL (2004) Myosin-1c, the hair cell's adaptation motor. *Annu Rev Physiol* 66:521-545.
16. Howard J & Hudspeth AJ (1988) Compliance of the hair bundle associated with gating of mechanoelectrical transduction channels in the bullfrog's saccular hair cell. *Neuron* 1(3):189-199.
17. Bozovic D & Hudspeth AJ (2003) Hair-bundle movements elicited by transepithelial electrical stimulation of hair cells in the sacculus of the bullfrog. *Proc Natl Acad Sci U S A* 100(3):958-963.
18. Martin P, Bozovic D, Choe Y, & Hudspeth AJ (2003) Spontaneous oscillation by hair bundles of the bullfrog's sacculus. *J Neurosci* 23(11):4533-4548.
19. Choe Y, Magnasco MO, & Hudspeth AJ (1998) A model for amplification of hair-bundle motion by cyclical binding of Ca2+ to mechanoelectrical-transduction channels. *Proc Natl Acad Sci U S A* 95(26):15321-15326.
20. Crawford AC, Evans MG, & Fettiplace R (1991) The actions of calcium on the mechano-electrical transducer current of turtle hair cells. *J Physiol (Lond)* 434:369-398.

695 21. Assad JA, Hacohen N, & Corey DP (1989) Voltage dependence of adaptation and active bundle
696   movement in bullfrog saccular hair cells. *Proc Natl Acad Sci U S A* 86(8):2918-2922.
697 22. Cheung EL & Corey DP (2005) Ca2+ Changes the Force Sensitivity of the Hair-Cell Transduction
698   Channel. *Biophys J*.
699 23. Ricci AJ & Fettiplace R (1997) The effects of calcium buffering and cyclic AMP on mechano-
700   electrical transduction in turtle auditory hair cells. *J Physiol (Lond)* 501(Pt 1):111-124.
701 24. Assad JA & Corey DP (1992) An active motor model for adaptation by vertebrate hair cells. *J
702   Neurosci* 12(9):3291-3309.
703 25. Effertz T, Becker L, Peng AW, & Ricci AJ (2017) Phosphoinositol-4,5-Bisphosphate Regulates
704   Auditory Hair-Cell Mechanotransduction-Channel Pore Properties and Fast Adaptation. *J
705   Neurosci* 37(48):11632-11646.
706 26. Dinklo T, Meulenberg CJ, & van Netten SM (2007) Frequency-dependent properties of a fluid
707   jet stimulus: calibration, modeling, and application to cochlear hair cell bundles. *J Assoc Res
708   Otolaryngol* 8(2):167-182.
709 27. Nam JH, Peng AW, & Ricci AJ (2015) Underestimated Sensitivity of Mammalian Cochlear Hair
710   Cells Due to Splay between Stereociliary Columns. *Biophys J* 108(11):2633-2647.
711 28. Corns LF, Johnson SL, Kros CJ, & Marcotti W (2014) Calcium entry into stereocilia drives
712   adaptation of the mechanoelectrical transducer current of mammalian cochlear hair cells. *Proc
713   Natl Acad Sci U S A* 111(41):14918-14923.
714 29. Crawford AC & Fettiplace R (1985) The mechanical properties of ciliary bundles of turtle
715   cochlear hair cells. *J Physiol (Lond)* 364:359-379.
716 30. Ricci AJ, Crawford AC, & Fettiplace R (2000) Active hair bundle motion linked to fast transducer
717   adaptation in auditory hair cells. *J Neurosci* 20(19):7131-7142.
718 31. Beurg M, Goldring AC, & Fettiplace R (2015) The effects of Tmc1 Beethoven mutation on
719   mechanotransducer channel function in cochlear hair cells. *J Gen Physiol* 146(3):233-243.
720 32. Corns LF, Johnson SL, Kros CJ, & Marcotti W (2016) Tmc1 Point Mutation Affects Ca2+
721   Sensitivity and Block by Dihydrostreptomycin of the Mechanoelectrical Transducer Current of
722   Mouse Outer Hair Cells. *J Neurosci* 36(2):336-349.
723 33. Beurg M, Nam JH, Crawford A, & Fettiplace R (2008) The actions of calcium on hair bundle
724   mechanics in mammalian cochlear hair cells. *Biophys J* 94(7):2639-2653.
725 34. Kennedy HJ, Crawford AC, & Fettiplace R (2005) Force generation by mammalian hair bundles
726   supports a role in cochlear amplification. *Nature* 433(7028):880-883.
727 35. Kros CJ*, et al.* (2002) Reduced climbing and increased slipping adaptation in cochlear hair cells
728   of mice with Myo7a mutations. *Nat Neurosci* 5(1):41-47.
729 36. Russell IJ, Richardson GP, & Kossl M (1989) The responses of cochlear hair cells to tonic
730   displacements of the sensory hair bundle. *Hear Res* 43(1):55-69.
731 37. Indzhykulian AA*, et al.* (2013) Molecular remodeling of tip links underlies mechanosensory
732   regeneration in auditory hair cells. *PLoS Biol* 11(6):e1001583.
733 38. Tobin M, Chaiyasitdhi A, Michel V, Michalski N, & Martin P (2019) Stiffness and tension
734   gradients of the hair cell's tip-link complex in the mammalian cochlea. *bioRxiv*:497222.
735 39. Vollrath MA & Eatock RA (2003) Time course and extent of mechanotransducer adaptation in
736   mouse utricular hair cells: comparison with frog saccular hair cells. *J Neurophysiol* 90(4):2676-
737   2689.
738 40. Beurg M, Fettiplace R, Nam JH, & Ricci AJ (2009) Localization of inner hair cell
739   mechanotransducer channels using high-speed calcium imaging. *Nat Neurosci* 12(5):553-558.
740 41. Strickholm A (1995) A supercharger for single electrode voltage and current clamping. *J
741   Neurosci Methods* 61(1-2):47-52.

742   42.   Ramunno-Johnson D, Strimbu CE, Fredrickson L, Arisaka K, & Bozovic D (2009) Distribution of
743   frequencies of spontaneous oscillations in hair cells of the bullfrog sacculus. *Biophys J*
744   96(3):1159-1168.

745